

Estimation of Constraint under Cyclic Loading on Cracked Components

M. Madia, S. Beretta
Politecnico di Milano, Milan, Italy

Abstract

The constraint plays an important role in the fatigue design of mechanical components. In particular, the global constraint factor α_g is the most used parameter in the field of fatigue to evaluate the level of constraint at the crack front and it is a crucial parameter in wide spread algorithms.

The present work aims to address how to obtain reliable values of constraint to employ in fatigue crack growth simulations, in order to improve the predictions of crack propagation models such as the Strip-Yield model.

A novel approach is presented for the calculation of the global constraint factor, based on the evaluation of local field parameters (J -integral, T -stress) and cyclic material properties. The model was set up on typical fracture mechanics and fatigue test specimens, then applied to the evaluation of the constraint state ahead of cracks in a railway axle.

1. Introduction

It is well known that the resistance against the ductile crack growth and propagation depends on the load conditions as well as on the geometrical configuration of the components. The discussion about the so-called *constraint effects* covered the last decades; many attempts were done to introduce a second parameter, which could quantify the level of constraint at the crack tip.

Historically, the approach to the role of constraint on crack propagation was developed following two different ways, one concerning with monotonic loading, whereas the second one is mostly employed in the field of fatigue.

The former could be regarded as a *local* approach, as it addresses the problem by the assessment of the constraint parameter (such as stress triaxiality h [1], T -stress [2,3,4], Q -stress [5,6,7] or A_2 [8,9]) directly ahead of the crack front, where the fracture occurs.

The latter is based on the evaluation of the global constraint parameter α_g introduced by Newman [10] and it is rather a *global* approach, as α_g is calculated as an average constraint value along the crack front. It is of some importance to emphasize that α_g was evaluated by Newman at the maximum stress (S_{max}) of the fatigue cycle. As aforementioned, α_g is a crucial parameter in fatigue crack growth and it is commonly adopted as constraint parameter in wide-spread fatigue crack growth algorithms such as the NASGRO equation [11] and the Strip Yield model (SY) [12].

The constraint plays an important role in the fatigue design of mechanical components. Previous works, carried out by the authors on different mild steels, addressed already the influence of constraint on fatigue strength in presence of inhomogeneities [13], on fitting crack growth data [14] and on modelling of fatigue thresholds for small cracks [15].

The difficulties associated to the calculation of the global constraint parameter α_g (mainly due to the computational effort) were overcome by means of a novel procedure [16,17] which employs the *local* approach (in the sense previously defined) to obtain reliable values of α_g . In particular, the assessment of the global constraint factor is based on the evaluation of local field parameters (*J*-integral, *T*-stress) and cyclic material properties. This approach was applied successfully to the evaluation of the constraint on a set of different fracture mechanics specimens and notched fatigue specimens, in case of two mild steels [16,18].

This paper addresses the transferability of the procedure from the specimens to the component in order to obtain reliable values of constraint for mechanical components in mild steel. In particular, the approach was employed to assess the state of constraint for a cracked railway axle made of A1N steel. The results allowed to compare the fatigue-crack growth behaviour obtained from the full-scale tests with the one derived from the typical fracture mechanics specimens.

2. Crack growth properties of A1N steel

The material analyzed in the present study is a mild carbon steel (named A1N) which is widely employed for manufacturing railway axles [19]. The basic mechanical properties of the material were already investigated by the authors [20] and are summarized in Table 1.

Table 1. Basic mechanical properties of A1N steel [20].

E [MPa]	$R_{p0.2}$ [MPa]	UTS [MPa]	E_{cyc} [MPa]	$R_{p0.05cyc}$ [MPa]	$R_{p0.2cyc}$ [MPa]
197500	388	591	200000	288	364

Of particular interest, for the sake of the present research, are the crack growth properties of the material. Crack growth and ΔK -decreasing tests were carried out on SENB specimens obtained from three different steel batches (more details about the tests are reported in [20]). Experimental data were also obtained from two full-scale crack propagation tests on axles under rotary bending ($R = -1$) [20]. The data in case of $R = -1$ are represented in Fig. 1, in which it is possible to appreciate a significant scale effect between small-scale and full-scale specimens, probably due to the different constraint at the crack tip. In light of this, further crack growth tests were carried out on a novel specimen (SENT with thickness equal to 20 mm and width equal to 50 mm, [21]), which was designed to have a state of constraint closer to the full-scale axle. The results obtained from the two tests performed with the novel specimen (Fig. 1) seem to match perfectly the crack growth behaviour of the full-scale tests, thus confirming the initial idea that

a different constraint condition is the reason for a different behaviour between SENB specimens and full-scale axles.

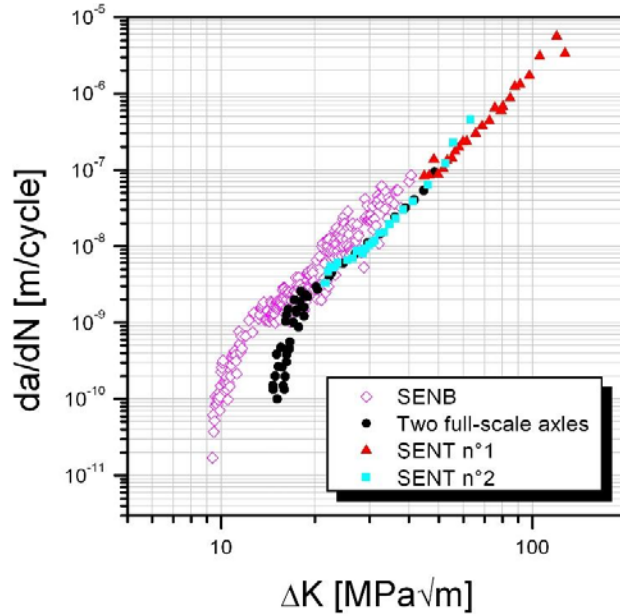


Fig. 1. Crack growth tests carried out on the A1N steel at $R = -1$.

3. Numerical methods

In order to confirm the experimental findings, the finite element method was employed (all the analysis were carried out by means of the commercial software ABAQUS[®] [22]) to study the state of constraint ahead of the crack front for the SENB and modified SENT specimen, as well as for the full-scale axle. The constraint values were then assessed in terms of global constraint factor α_g by means of the novel procedure described in [16,17].

It is important to emphasize that, in case of real components subjected to cyclic loading at $R = -1$, the maximum stress (S_{max}) of the fatigue cycle can be approximated by the cyclic curve of the material.

3.1. Finite element analysis

The finite element analysis were carried out on three-dimensional models in order to reproduce the real state of stress along the crack front of both specimens and full axle. Different loading conditions and crack dimensions were modelled, as the constraint value is extremely sensitive to these parameters, in particular:

- SENT specimens with three different crack length (8, 14 and 20 mm), subjected to five remote stresses (55, 70, 82.5, 96.25 and 110 MPa);

- SENB specimens with crack lengths equal to 10 mm and 13 mm (notch + crack), subjected to five bending moments (17.4, 26.1, 30, 43.4 and 47 Nm). In case of the model with crack depth equal to 10 mm, a further bending moment of 69.8 Nm was used;
- full-axle with three different shallow cracks ($a/b = 0.2$ and $a/D = 0.025, 0.050, 0.075$; a is the crack depth, D the diameter of the axle at the place where the crack is set, a/b is the aspect ratio of the crack) and vertical load of 196.2 kN applied at each side of the axle, at the middle section of the bearing journal.

It was taken advantage of all the possible symmetries for reducing the computational effort and isoparametric 3D elements were employed (more details about the numerical procedures can be found in [16]). Two typical meshes are shown in Fig. 2, in particular, Fig. 2.a refers to the SENB specimen, whereas Fig. 2.b shows the mesh used for the full axle model. As the accuracy of the results of the finite element analysis is the main issue to obtain reliable constraint values, the mesh was highly refined within a distance larger than a plastic radius r_p along the crack front (the minimum size of the elements along the crack front was set equal to $0.625 \mu\text{m}$ in case of the SENB specimen), in order to catch precisely the state of stress and the plastic zone size ahead of the crack front.

The elastic-plastic material response was modelled by the multiaxial expression of the Ramberg-Osgood relationship [22].

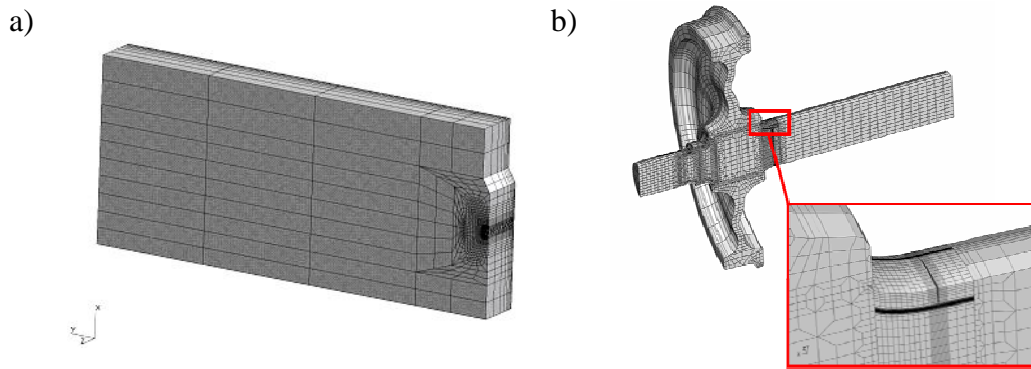


Fig. 2. Typical meshes employed in the finite element analysis: a) SENB specimen; b) full-axle with a magnification of the mesh refinement ahead of the crack front.

3.2. Assessment of the global constraint factor α_g

According to Newman [10], the global constraint factor at S_{max} is defined as follows:

$$\alpha_g = \frac{1}{A_T} \sum_{m=1}^M \left(\frac{\sigma_y}{\sigma_0} \right)_m A_m \quad (1)$$

where A_m is the projected area of a yielded element m onto the ligament, $(\sigma_y/\sigma_0)_m$ is the opening stress for the element m normalized by the yielding parameter σ_0 and A_T is the total projected area of the M elements which have yielded.

The expression given by Eq. (1) puts light on the common difficulties associated to the correct assessment of the constraint values: i) α_g is strongly dependent on the precise evaluation of the opening stresses σ_y ; ii) the numerical procedure is time-consuming due to the computational effort (highly refined mesh) and to the post-processing of the finite element data. In order to overcome these problems, a novel procedure was developed [16,17], the main features of which can be summarized as follows:

- the opening stresses (crack-tip fields) are represented by means of the J - A_2 theory, which proved to be extremely efficient for each loading (tension or bending) and geometrical (SENT, SENB and notched bars) configuration (see Fig. 3) [8,9,16,17];
- the value of the second parameter A_2 can be expressed as a function of the elastic T -stress under the assumption of small scale yielding [16,17];
- the plastic zone size is assessed through finite element calculations or invoking the expression of the plastic radius r_p under small scale yielding condition [23].

The final expression of the global constraint factor, if r_p is assessed according to Guo [23], is given by the following system of equations:

$$\left\{ \begin{array}{l} \alpha_g = \frac{1}{A_T} \int_{-B/2}^{B/2} \int_{2J/\sigma_0}^{r_p} \frac{1}{A_1} \left[\left(\frac{r\sigma_0}{J} \right)^{s_1} \tilde{\sigma}_{\theta=0}^{(1)} + A_2(T) \left(\frac{r\sigma_0}{J} \right)^{s_2} \tilde{\sigma}_{\theta=0}^{(2)} + \right. \\ \left. + A_2^2(T) \left(\frac{r\sigma_0}{J} \right)^{s_3} \tilde{\sigma}_{\theta=0}^{(3)} \right] dr dz \\ r_p = \frac{\pi}{8} \left(\frac{K_{max}}{\alpha_g \sigma_0} \right)^2 \end{array} \right. \quad (2) \quad (3)$$

In Eq. (2), B is to be intended as the thickness of the specimen or the length of the crack front in case of surface cracks in components, T is the elastic T -stress, J is the J -integral, whereas the other quantities refer to the J - A_2 theory (more details can be found in [8,9]). The values of the constants in Eq. (2) for the material A1N are reported in [16]. In Eq. (3), K_{max} is the maximum value of the stress intensity factor.

The main feature of the novel procedure given by Eqs. (2) and (3) is that the global constraint value is a function of the geometry, material constants and two quantities (J -integral and T -stress) which don't need an extremely refined mesh to be assessed by finite elements.

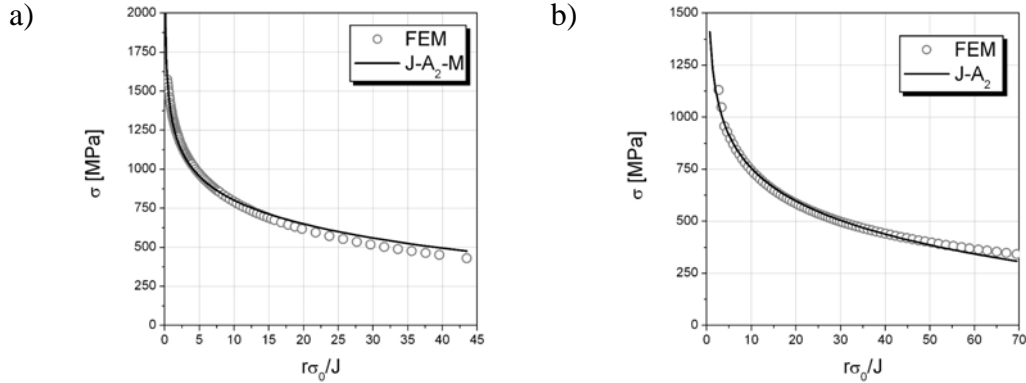


Fig. 3. Representation of the opening stresses by means of the $J-A_2$ theory: a) middle plane of the SENB specimen loaded with 69.8 Nm; b) middle plane of the SENT specimen with 14 mm crack length and remote stress equal to 110 MPa.

4. Results and discussion

The calculation of the global constraint factor was carried out employing both the procedures explained in the foregoing paragraph: in case of the small-scale specimens (SENB, SENT) the plastic zone extension r_p was assessed by the finite element results, whereas in case of the full-scale axle it was obtained by means of the Guo's expression.

The α_g values, reported in Fig. 4, put in evidence a different behaviour for each kind of specimen. The SENB specimen is characterized by higher constraint values compared to those obtained for the full-scale axle, which gives the explanation for the different crack growth behaviour shown in Fig. 1. In fact, for a given applied load, higher constraint values yield higher opening stresses ahead of the crack front, thus a higher crack-growth rate and a lower threshold. The analysis carried out on the modified SENT specimens confirm the initial idea of a constraint state much closer to the real full-axle conditions.

The different constraint condition between the SENB and SENT specimens can be also put in evidence by the values of the constraint parameter A_2 . In particular, Fig. 5 shows the trend of A_2 through the thickness of SENB ($a = 10$ mm, 69.8 Nm) and SENT ($a = 8$ mm, 110 MPa) specimens.

Further findings were obtained by SY simulations, considering α_g equal to 2.7, which represents the average of the estimated values for the full-axle. Fig. 6 shows that the results of the SY simulation yields a very good approximation of the experimental crack growth data.

It is then possible to conclude that the novel procedure for the calculation of the global constraint factor is able to yield reliable α_g values also for surface cracks in a real component. Moreover, the global constraint provides a reasonable explanation of the fatigue crack growth behaviour of the A1N steel for different geometrical and loading configurations.

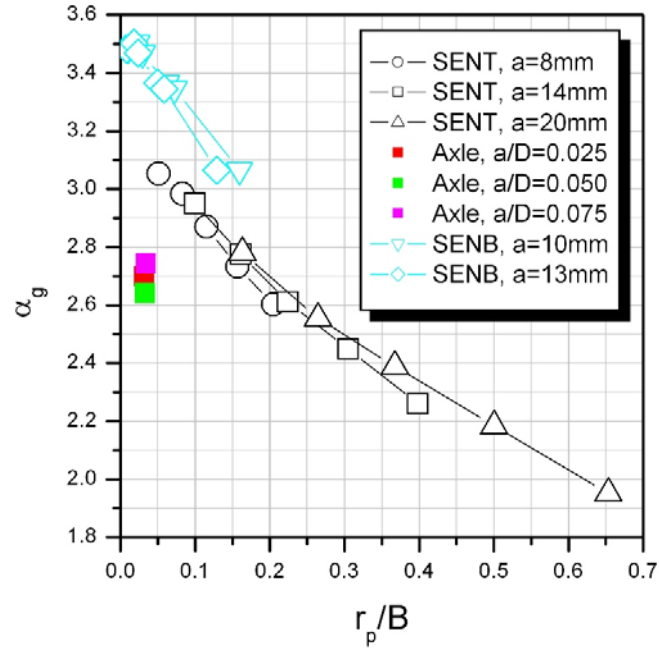


Fig. 4. Global constraint values for each geometrical and loading configuration.

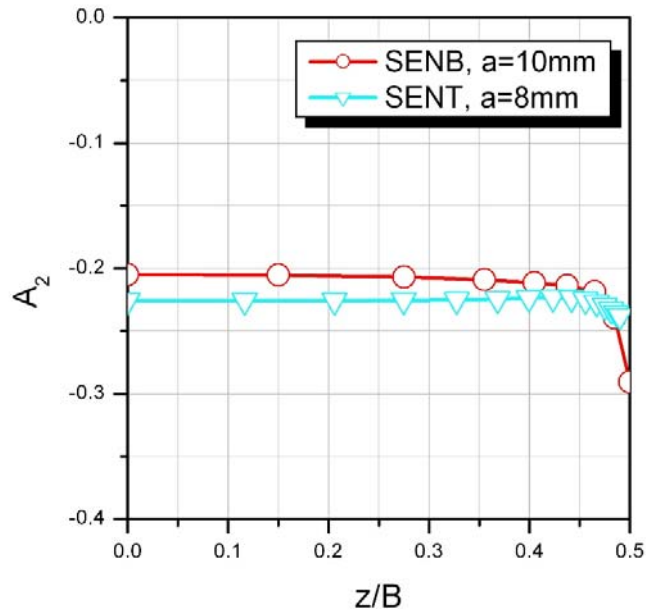


Fig. 5. Values of the constraint parameter A_2 through the thickness of SENB ($a = 10$ mm, 69.8 Nm) and SENT ($a = 8$ mm, 110 MPa) specimens.

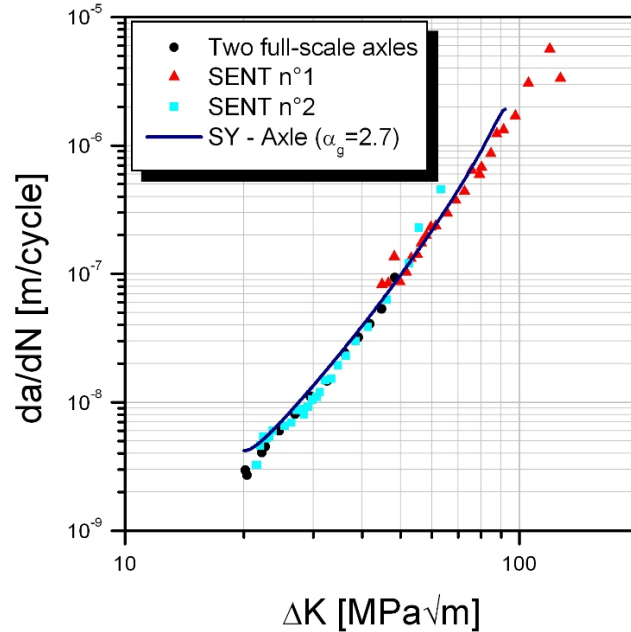


Fig. 6. Comparison between the results of the SY simulation and the experimental crack growth data.

5. References

- [1] H. Yuan, W. Brocks, Quantification of constraint effects in elastic-plastic crack front fields, *J Mech Phys Solids* 46 (2) (1998) 219-241
- [2] C. Betegon, J.W. Hancock, Two-parameter characterization of elastic-plastic crack-tip fields, *J Mech Phys Solids* 58 (1991) 104-110
- [3] A.M. Al-Ani, J.W. Hancock, J-dominance of short cracks in tension and bending, *J Mech Phys Solids* 39 (1991) 23-43
- [4] Z.Z. Du, J.W. Hancock, The effect of non-singular stresses on crack-tip constraint, *J Mech Phys Solids* 39 (1991) 555-567
- [5] S.M. Sharma, N. Aravas, Determination of higher order terms in asymptotic elastoplastic crack tip solutions, *J Mech Phys Solids* 39 (8) (1991) 1043-1072
- [6] N.P. O'Dowd, C.F. Shih, Family of crack-tip fields characterized by a triaxiality parameter – I. Structure of fields, *J Mech Phys Solids* 39 (8) (1991) 989-1015
- [7] N.P. O'Dowd, C.F. Shih, Family of crack-tip fields characterized by a triaxiality parameter – II. Fracture applications, *J Mech Phys Solids* 40 (5) (1992) 939-963

- [8] S. Yang, Y.J. Chao, M.A. Sutton, Higher order asymptotic crack tip fields in a power-law hardening material, *Eng Fract Mech* 45 (1) (1993) 1-20
- [9] Y. Kim, X.K. Zhu, Y.J. Chao, Quantification of constraint on elastic-plastic 3D crack front by the J - A_2 three-term solution, *Eng Fract Mech* 68 (2001) 895-914
- [10] J.C. Newman Jr, C.A. Bigelow, K.N. Shivakumar, Three-Dimensional Elastic-Plastic Finite-Element Analyses of Constraint Variations in Cracked Bodies, *Eng Fract Mech* 46 (1993) 1-13
- [11] J.C. Newman Jr, A crack opening stress equation for fatigue crack growth, *Int J Fract* 24 (1984) R131-R135
- [12] J.C. Newman Jr, A crack closure model for predicting fatigue crack growth under aircraft spectrum loading, in: J.B. Chang, C.M. Hudson (Eds.), *Methods and models for predicting fatigue crack growth under random loading*, ASTM STP 748, American Society for Testing and Materials, 1981, pp.53-84
- [13] S. Beretta, M. Carboni, M. Madia, Fatigue Strength in Presence of Inhomogeneities: Influence of Constraint, *J ASTM Int* 3 (4) (2006) 1-11
- [14] M. Carboni, M. Madia, The Influence of Constraint on Fitting Crack Growth Data, in: E. E. Gdoutos (Ed.), *Proceedings of the 16th European Conference of Fracture*, Springer, Dordrecht, 2006, pp. 231-232
- [15] S. Beretta, M. Carboni, M. Madia, Cyclic stress ahead of non-propagating cracks, in: *Proceedings of MatModels2007*, Hamburg, 2007
- [16] M. Madia, Effect of constraint on crack propagation in mechanical components, Ph.D. thesis, Milan, 2008
- [17] M. Madia, S. Beretta, Assessment of the global constraint by a local approach, in preparation
- [18] M. Madia, Analysis of the cyclic stress ahead of small cracks at $R = -1$, in: J. Pokluda, P. Lukáš, P. Šandera, I. Dlouhý (Eds.), *Proceedings of the 17th European Conference of Fracture*, VUTIUUM, Brno, 2008, p. 161
- [19] EN13261, Railway applications – Wheelsets and bogies – Axles – Product requirements, BSI, 2003
- [20] S. Beretta, M. Carboni, S. Cantini, A. Ghidini, Application of fatigue crack growth algorithms to railway axles and comparison of two steel grades, *Journal of Rail and Rapid Transit* 218 (2004) 317-326.

[21] S. Beretta, M. Carboni, M. Madia, Analysis of Crack Growth at $R = -1$ Under Variable Amplitude Loading on a Steel for Railway Axles, J ASTM Int 5 (7) (2008) 1-13

[22] ABAQUS ver.6.5, Reference manual, HKS, 2005

[23] W. Guo, Three-dimensional analyses of plastic constraint for through-thickness cracked bodies, Eng Fract Mech 62 (1999) 383-407